Chinese Chemical Letters 37 (2026) 112462

Contents lists available at ScienceDirect

Chinese Chemical Letters

journal homepage: www.elsevier.com/locate/cclet

Integrated electrochemical and catalytic system with metal-free CNT membrane electrode for efficient aniline degradation *via* peracetic acid activation

Wentian Zheng[a], Jiachen Wang[b], Yifan Ren[b,*], Yanbiao Liu[a,b,*]

[a] College of Environmental Science and Engineering, Donghua University, Shanghai 201620, China
[b] School of Environmental Science and Technology, Key Laboratory of Industrial Ecology and Environmental Engineering (Ministry of Education), Dalian University of Technology, Dalian 116024, China

ARTICLE INFO

Article history:
Received 21 October 2025
Revised 28 November 2025
Accepted 23 January 2026
Available online 23 January 2026

Keywords:
Peracetic acid
Electrocatalysis
Organic radicals
Aniline elimination
Carbon nanotube

ABSTRACT

This study introduces a functionalized carbon nanotube (CNT) membrane electrode integrated into an electrochemical system for the efficient activation of peracetic acid (PAA) and the enhanced degradation of aniline (AN). The system achieves a remarkable 95.5 % removal of AN within 120 min, significantly outperforming individual electrochemical and catalytic processes. Kinetic analysis reveals a pseudo-first-order rate constant of 2.41×10^{-2} min^{-1}, representing 12.7-fold and 2.3-fold enhancement compared to electrochemical and catalytic systems alone. The novel approach exploits the synergistic effects of an applied electric field and the functionalized surface of CNT, with C–OH groups identified as the primary active sites for radical generation. The degradation proceeds *via* dual pathways: A dominant surface-mediated route involving reactive R–O$^{\bullet}$ radicals, and an electron-transfer pathway, which is more prominent in the absence of an electric field. The applied voltage (2.0 V) shifts the system to favor the radical-mediated pathway, significantly improving degradation efficiency. The system also demonstrates excellent stability, maintaining over 90 % efficiency across multiple cycles and robust performance in complex water matrices. Furthermore, anti-fouling tests and XDLVO theory affirmed that the H-CNT membrane possesses exceptional stability and anti-fouling properties. Life cycle assessment further highlights the reduced environmental footprint of the proposed technology. Overall, this work provides essential insights into the carbon-catalyzed PAA activation mechanism and presents a promising strategy for sustainable wastewater treatment, effectively reducing the toxicity of degradation intermediates.

© 2026 Published by Elsevier B.V. on behalf of Chinese Chemical Society and Institute of Materia Medica, Chinese Academy of Medical Sciences.

Advanced oxidation processes (AOPs) have become essential tools for wastewater decontamination due to their capacity to effectively degrade a range of organic pollutants through the generation of reactive oxygen species (ROS), such as hydroxyl radical ($HO^{\bullet}$), sulfate ($SO_4^{\bullet-}$), and peroxide ion radicals ($O_2^{\bullet-}$) [1–3]. However, the efficiency of AOPs is often limited by the activation of oxidants, which typically requires significant external energy input or catalyst intervention. For instance, while persulfate-based AOPs have been extensively investigated, their practical application faces challenges related to high energy consumption and potential metal leaching from catalyst systems [4,5]. In contrast, peracetic acid (PAA, $CH_3C(O)OOH$), a relatively low-energy oxidant with a peroxide bond dissociation energy of 159 kJ/mol, has emerged as a viable alternative due to its ability to generate highly reactive radicals, such as acetoxyl radical ($CH_3COO^{\bullet}$) and acetylperoxy radical ($CH_3C(O)OO^{\bullet}$), which exhibit strong reactivity toward electron-rich organic pollutants [6,7]. The residual PAA and its decomposition byproducts can also serve as carbon sources for downstream biological treatment processes, adding to the overall sustainability of the system.

Despite the advantage of PAA, its activation has traditionally relied on energy-intensive methods such as ultraviolet irradiation [8] and thermal activation [9,10], which suffer from low efficiency. Furthermore, transition metals (*e.g.,* Fe, Co, Mn) [11–13], although effective, often face issues related to catalyst recovery and potential metal ion leaching in both homogeneous and heterogeneous systems [14]. As a result, there is a growing interest in using carbon-based materials, including activated carbon fibers (ACF) [15], reduced graphene oxide (rGO) [16] and carbon nanotubes (CNT) [17], as alternatives to metal catalysts. These materials are environmen-

* Corresponding authors.
E-mail addresses: yifanren@dlut.edu.cn (Y. Ren), yanbiaoliu@dhu.edu.cn (Y. Liu).

https://doi.org/10.1016/j.cclet.2026.112462
1001-8417/© 2026 Published by Elsevier B.V. on behalf of Chinese Chemical Society and Institute of Materia Medica, Chinese Academy of Medical Sciences.

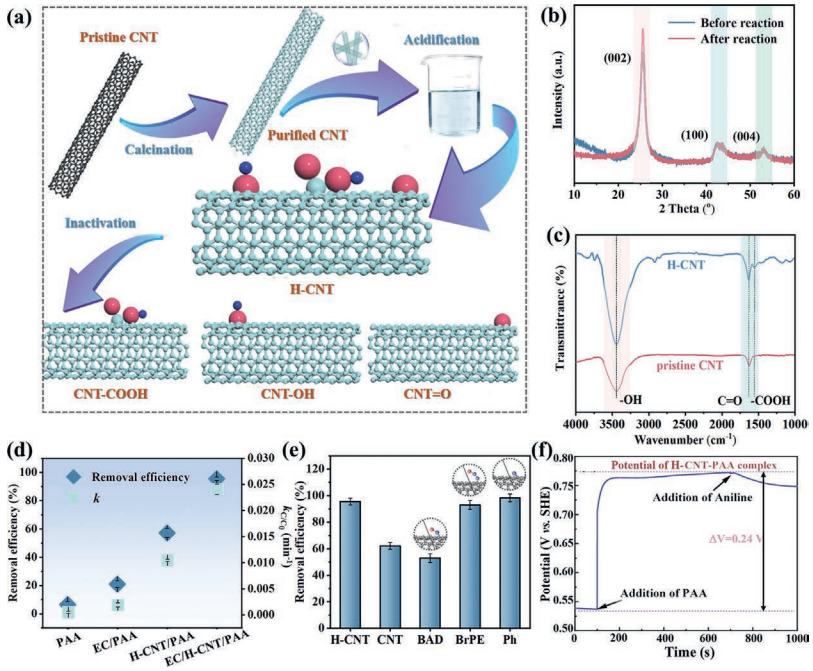


Fig. 1. (a) Schematic illustration of the fabrication process for the CNT membrane functionalized with –OH/–C=O/–COOH. (b) XRD patterns of the H-CNT before and after the reaction. (c) FTIR spectra of the CNT before and after acidification treatment. (d) AN degradation efficiency in different systems. (e) Effect of quenching different oxygen groups in H-CNT on AN degradation. (f) Quantitative determination of contribution for AN removal in different conditions. Condition: $[AN]_0 = 0.04$ mmol/L, $[PAA]_0 = 2.0$ mmol/L, $[Ph]_0 = [BAD]_0 = [BrPE]_0 = 50$ mmol/L, initial pH 7, voltage = 2.0 V, flow rate = 3.0 mL/min.

tally friendly, exhibit high chemical stability, and possess tunable surface properties that can enhance PAA activation [18].

Among various carbon-based materials, CNT stand out as candidates for electrode materials due to their excellent electrical conductivity, remarkable chemical stability, and high specific surface area [19,20]. However, the catalytic activity of pristine CNT is limited, and strategies to enhance their ability to activate PAA are needed. This study introduces a functionalized CNT membrane electrode that integrates electrochemical and catalytic processes for efficient PAA activation and the removal of aniline (AN), a common and persistent environmental pollutant. By functionalizing CNT with oxygen-containing groups (–OH, –C=O, and –COOH), we enhance their catalytic performance and facilitate PAA activation. This work investigates the role of surface functional groups and the applied electric field in regulating two distinct yet synergistic reaction pathways: A surface-mediated radical pathway and an electron-transfer pathway. Through systematic experiments, we aim to provide a deeper understanding of the mechanisms behind CNT-catalyzed PAA activation and offer insights into the practical application of this integrated electrochemical system for the treatment of refractory organic pollutants in real-world wastewater scenarios.

Detailed information regarding the chemicals and materials was provided in Text S1 (Supporting information). Deionized (DI) water, with a resistivity of ≥18.2 MΩ cm, was obtained from a Milli-Q Direct 8 system (Millipore, USA). The fabrication of the functionalized CNT membrane electrode was carried out through a multistep process (Fig. 1a). Raw CNT (2 g) was first purified by calcination in a tube furnace. The temperature was gradually raised from room temperature to 400 °C at a heating rate of 5 °C/min and maintained for 1 h to remove residual amorphous carbonaceous impurities [12]. The purified CNT was then functionalized by refluxing in 250 mL of concentrated HNO_3 (68 %–70 %) at 70 °C for 15 h under vigorous stirring with a condenser attached. Under this mild refluxing condition, the carbonyl, hydroxyl, and carboxyl groups were primarily introduced onto the outer walls of the CNT [21]. After cooling to room temperature, the resulting product (denoted as H-CNT) was filtered through a 0.45 μm polytetrafluoroethylene (PTFE) membrane and thoroughly washed with DI water until the filtrate reached a neutral pH. The functionalized H-CNT (25 mg) was then dispersed in 1-methyl-2-pyrrolidinone and sonicated for 40 min to ensure uniform suspension. Finally, this suspension was vacuum-filtered onto a PTFE membrane to obtain the freestanding H-CNT membrane electrode. Detailed characterization methods are available in Text S2 (Supporting information).

Prior to electrochemical degradation experiments, adsorption saturation was achieved by recirculating a 0.04 mmol/L pollutant solution through the membrane at 3 mL/min for 2 h. Degradation experiments were performed in both batch and flow-through electrochemical reactors to evaluate the performance of the integrated electrochemical system for AN removal. In batch mode, 50 mL of a mixed solution containing AN (0.04 mmol/L) and PAA (2.0 mmol/L) was placed in a beaker equipped with the CNT membrane electrode as the anode and a titanium plate as the cathode. The solution pH was adjusted using 10 mmol/L NaOH or H_2SO_4, and the system was operated at ambient temperature. The applied voltage was controlled using a high-precision DC power supply (DH1766A-1, China). For the flow-through experiments, a custom-made electrochemical reactor was employed, consisting of the H-CNT membrane electrode as the anode and a perforated titanium plate as the cathode. The mixed solution (50 mL) was continuously circulated through the reactor at a flow rate of 3 mL/min using a peristaltic pump (ISM833C, Ismatec, Switzerland). The applied voltage was set to 2.0 V. Throughout the experiments, 1 mL of solution was collected at regular intervals and filtered through a 0.22 μm polyester membrane before analysis. Each degradation experiment was performed in triplicate, and the results were presented as mean values with corresponding standard deviations.

To determine optimal operational parameters, the effects of PAA concentration (0–2 mmol/L), solution pH (3.5–10), applied voltage (0–2.5 V) and flow rate (1.5–4.5 mL/min) on the pollutant degradation kinetics were systematically investigated. Moreover, the in-

fluence of typical inorganic anions (*e.g.,* HCO_3^-, HPO_4^{2-}, and Cl^-) and humic acid (HA) on the AN degradation was evaluated. To assess the versatility of the electrochemical system, organic degradation experiments were extended to other refractory organic contaminants, including sulfamethoxazole (SMX), bisphenol A (BPA), tetracycline (TC), benzoic acid (BA), and nitrobenzene (NB). The robustness and stability of the system were further evaluated under complex operational scenarios.

The concentration of the PAA was determined by iodometric titration [18], while residual PAA concentration during reaction was measured using the *N*,*N*-diethyl-*p*-phenylenediamine sulfate colorimetric method (Text S3 in Supporting information) [22]. High-performance liquid chromatography (HPLC; Shimadzu LC-20A, Japan) was used to quantify the concentrations of target pollutants, with detailed operational parameters summarized in Table S1 (Supporting information). Intermediate products generated during AN degradation were analyzed by ultrahigh-performance liquid chromatography coupled with quadrupole time-of-flight mass spectrometry (UPLC-QTOF-MS; Agilent 6500 LC/Q-TOF). To identify the ROS involved in the degradation process, electron paramagnetic resonance spectroscopy (EPR; Bruker EMXnano) was conducted using 5,5-dimethyl-1-pyrroline *N*-oxide (DMPO) as the spin trap for $HO^•$ and $R–O^•$. All degradation kinetics followed *pseudo*-first-order models, as detailed in Text S4 (Supporting information).

The prepared H-CNT membrane was first characterized to elucidate its surface morphology and chemical properties. As displayed in Fig. S1 (Supporting information), the field emission scanning electron microscope (FESEM) image revealed a smooth and homogeneous surface with uniform diameters ranging from 10 nm to 20 nm, indicating the high quality of the functionalized H-CNT. Notably, the CNT were observed with closed ends, and no substantial rupture of the tubular structure was detected (Fig. S2 in Supporting information). This intact morphology suggested that the acidification process under our moderate conditions preferentially functionalized the outer walls without severely compromising the structural integrity or extensively attacking the less accessible inner channel [14]. X-ray diffraction (XRD) analysis confirmed the crystalline structure of the H-CNT, showing prominent peaks at approximately 25°, 43°, and 53°, corresponding to the (002), (100), and (004) crystallographic planes of graphite, respectively (Fig. 1b). FETEM further validated the graphitic nature of the H-CNT, revealing well-resolved lattice fringes with a measured *d*-spacing of 0.34 nm (Fig. S3 in Supporting information), characteristic of the (002) plane. Additionally, Fourier transform infrared (FTIR) spectroscopy was performed to compare the CNT before and after acidification. The results confirmed the successful functionalization, as evidenced by a marked enhancement of the absorption bands associated with –OH (3200–3600 cm^{-1}), C=O (1633 cm^{-1}), and –COOH (1558 cm^{-1}) in the acid-treated H-CNT membrane (Fig. 1c). This provides direct evidence for the effective introduction of oxygen-containing functional groups during the acidification process.

The catalytic performance of the H-CNT membrane was systematically evaluated by investigating the degradation of AN, selected as a model refractory pollutant due to its environmental persistence and representative aromatic amine structure. To assess the efficacy of the integrated system, we compared four experimental steps: (1) PAA alone, (2) electrochemical oxidation of PAA (EC/PAA), (3) H-CNT-activated PAA system (H-CNT/PAA), and (4) the integrated electrochemical H-CNT-activated PAA system (EC/H-CNT/PAA). As shown in Fig. 1d, the PAA-only system demonstrated limited oxidative capacity, achieving merely 6.5% AN removal after 120 min. This low removal rate can be attributed to the relatively weak reactivity of non-activated PAA, which undergoes limited decomposition under ambient conditions. In contrast, the EC/PAA system, which employed electrochemical oxidation with Na_2SO_4 as the electrolyte, resulted in a significant increase in AN removal to 21.0%. This improvement is attributable to the generation of reactive species at the electrode surface *via* electrochemical processes, which facilitated the oxidation of AN [23]. Further enhancement was observed when H-CNT was incorporated into the system. The H-CNT/PAA system achieved 57.2% AN removal, highlighting the crucial role of oxygen-functionalized H-CNT in mediating electron transfer and facilitating PAA-derived radical generation. The most remarkable enhancement was observed in the integrated EC/H-CNT/PAA system, which achieved 95.5% AN removal within 120 min when a 2.0 V external voltage was applied. This exceptional performance underscores the synergistic effects between the applied electric field and the oxygen-functionalized surface of the CNT, which accelerates both electron transfer and ROS generation.

Kinetic analysis of the degradation process revealed a pseudo-first-order rate constant of 2.41×10^{-2} min^{-1} for the EC/H-CNT/PAA system, which was 12.7 and 2.3 times higher than the corresponding rate constants for the EC/PAA and H-CNT/PAA systems, respectively. This marked acceleration in reaction rate further substantiates the synergistic effect of electrochemical activation and CNT functionalization in enhancing the PAA activation process. The observed rate constant provides compelling evidence for the cooperative role of electrochemical stimulation and surface-functionalized catalysis in facilitating advanced oxidation reactions. In addition, the exceptional stability of the H-CNT membrane was corroborated by XRD analysis conducted before and after the reaction (Fig. 1b). The absence of significant changes in the characteristic peaks indicates negligible catalyst passivation and attests to the robust structural and chemical stability of the H-CNT under prolonged operational conditions.

To gain a deeper understanding of the degradation mechanism, we systematically compared the catalytic performance of functionalized H-CNT with that of pristine CNT. As illustrated in Fig. 1e, the H-CNT achieved a remarkable degradation efficiency of 95.5%, substantially higher than the 62.2% efficiency of pristine CNT, underscoring the crucial contribution of surface functionalization to the catalytic enhancement. To further elucidate the individual roles of the oxygen functional groups, we performed selective blocking experiments using chemical titrations [24]. Specifically, phenylhydrazine (Ph), benzoyl anhydride (BAD), and 2-bromo-1-phenylethanone (BrPE) were used to selectively mask C=O, C–OH, and –COOH groups, respectively (Fig. 1e). The results revealed that blocking C–OH groups with BAD led to a dramatic reduction in AN degradation efficiency, from 95.5% to 53.0%. In contrast, blocking the –COOH (with BrPE) or C=O (with Ph) had negligible effects on the degradation process. These findings definitively identify C–OH as the primary active site responsible for activation of PAA and subsequent degradation of AN.

In addition to the surface functional groups, electron transfer through the CNT network plays a critical role in PAA activation. Previous studies have shown that the conjugated π-system of CNT facilitates electron transfer, which is essential for the activation of PAA to form highly reactive radicals [3]. To directly investigate the electron transfer process, we employed a suite of electrochemical characterization techniques, including open circuit potential (OCP) monitoring, linear sweep voltammetry (LSV), and chronoamperometry (*I*-*t*) measurements (Fig. 1f, Figs. S4 and S5 in Supporting information). These methods provided real-time evidence for the existence and dynamics of the electron transfer pathway during the catalytic process. As shown in Fig. 1f, the OCP measurements revealed that the introduction of PAA to the H-CNT caused an immediate positive potential shift, indicating the chemical adsorption of PAA on the H-CNT surface. Upon the addition of AN, a pronounced negative shift was observed, which was indicative of spontaneous electron donation from AN to the PAA-adsorbed H-CNT surface. This result suggested that AN served as the electron donor, providing the necessary electrons to reduce the PAA-activated surface

complex (H-CNT-PAA*). The formation of the H-CNT-PAA* complex is a key intermediate in the electron transfer pathway, facilitating the activation of PAA and subsequent radical generation.

Further electrochemical analysis using *I-t* and LSV measurements supported these findings. The *I-t* curves showed an initial increase in current upon the introduction of PAA, corresponding to the formation of the H-CNT-PAA* complex. A subsequent sharp increase in current was observed upon adding AN, reflecting the intense electron transfer from AN to the H-CNT surface (Fig. S5 in Supporting information). The rapid electron flow through the CNT network was crucial for the reduction of the H-CNT-PAA* complex, thereby enabling efficient pollutant degradation. These electrochemical signatures provided strong evidence for the electron transfer mechanism, where the CNT acted as an efficient electron conduit, enabling the activation of PAA and the degradation of AN. To complement the electrochemical findings, Raman spectroscopy (Fig. S6 in Supporting information) was employed to confirm the formation and consumption of the H-CNT-PAA* complex during the catalytic process. The introduction of PAA resulted in the appearance of a distinct peak at 889 cm^{-1}, attributed to the characteristic vibration of the H-CNT-PAA* complex. This peak vanished immediately after the AN introduction, confirming that the H-CNT-PAA* complex was consumed upon electron transfer from AN. This provides direct spectroscopic evidence that the degradation process is mediated by the electron transfer to this specific surface complex (H-CNT-PAA*). Complementarily, the dynamic aspect of this electron transfer was quantified by LSV, which revealed a remarkable synergistic current enhancement in the simultaneous presence of PAA and AN. This cooperative effect substantiates that H-CNT mediates an efficient electron-transfer pathway, functioning as an active electron-conduction channel that facilitates the oxidation of AN by PAA.

To quantitatively evaluate the respective contributions of these parallel reaction mechanisms under different operational conditions, systematic experiments were conducted both with and without the application of an external voltage. In the absence of an applied voltage, the electron-transfer pathway *via* the H-CNT-PAA* complex was found to contribute 64.1 % to the overall AN degradation. This pathway operated predominantly through the conjugated π-system of H-CNT, where the favorable energy alignment between HOMO of AN and the LUMO of H-CNT-PAA* complex facilitated spontaneous electron transfer, even without the need for external energy input [25]. When C–OH groups on the H-CNT surface were selectively blocked, the contribution of the electron-transfer pathway increased substantially to 84.5 %, further demonstrating the self-sufficient nature of this electron-transport mechanism (Fig. 2a). The introduction of a 2.0 V external potential fundamentally altered the catalytic landscape. Under electrochemical conditions, surface-mediated oxidation involving the C–OH became the dominant pathway, contributing 66.9 % of the total activity. The applied electric field induced significant interfacial charge polarization that preferentially stabilized the transition state for PAA decomposition at C–OH sites, thereby substantially lowering the activation energy barrier for surface-mediated reactions [26]. In contrast, when C–OH were quenched under electrochemical conditions, the overall degradation efficiency dropped significantly to 61.2 %. These findings provided compelling evidence for the indispensable role of C–OH group in the field-enhanced catalytic mechanism, as their presence is crucial for maintaining the efficiency of the integrated system. The distinct quantitative differences in pathway contributions, specifically 66.9 % for surface-mediated oxidation under applied potential compared to 64.1 % for electron transfer without the external voltage, revealed how operational conditions could dictate the dominant reaction mechanism through fundamental electronic interactions. This mechanistic duality originated from the unique electronic structure of H-CNT, where the graphitic basal plane provided an efficient electron conduction pathway while oxygen functional groups offered specifically tunable active sites with modifiable energy states. The electric field preferentially activated functionalized edges through controllable charge polarization, while simultaneously preserving the intrinsic electron-transfer capability of the conjugated carbon framework, revealing a sophisticated cooperative mechanism where both pathways can operate in concert, with their relative dominance modulated by the available energy input.

To gain atomic-level insights into the reaction mechanism, density functional theory calculations were performed to elucidate the fundamental differences between CNT and CNT–OH in activating PAA (Figs. 2b and c, Text S5 in Supporting information). The results demonstrated that the adsorption energy of PAA on CNT–OH (−1.29 eV) was significantly stronger than that on CNT (−1.04 eV), confirming that the C–OH group acted as a superior anchoring site that enriched the reactant concentration on the surface. We further calculated the reaction energy barrier for O–O bond cleavage in PAA, a key descriptor for evaluating reaction feasibility. The calculated reaction energy barrier for the O–O bond cleavage in PAA revealed a substantially lower activation barrier on the CNT–OH surface. This result indicated that the C–OH groups not only enhanced the adsorption of PAA but also fundamentally accelerated its activation by lowering the energy barrier for radical generation. The dual functionality of CNT–OH, characterized by stronger adsorption and a substantially reduced activation barrier, collectively directs the reaction toward the radical pathway. In contrast, the pristine CNT, with weaker adsorption and a higher activation barrier for O–O cleavage, preferentially stabilizes the CNT-PAA* complex and favors the non-radical electron transfer pathway. Thus, the C–OH group was unequivocally identified as the multifunctional active site responsible for both the effective capture and activation of PAA, driving the reaction toward a radical-mediated degradation pathway.

To further identify reactive radicals generated, electron paramagnetic resonance (EPR) spectroscopy was performed using DMPO and TEMP as spin-trapping agents for detecting radicals and singlet oxygen ($^1O_2$), respectively (Figs. S7 and S8 in Supporting information). Control experiments, conducted in the absence of H-CNT membrane electrode, showed no significant EPR signals, confirming that spontaneous radical generation from PAA decomposition did not occur without the CNT catalyst. In contrast, when the H-CNT was introduced into the system, distinct signals for DMPO-$HO^{\bullet}$ and DMPO-$RO^{\bullet}$ adducts were observed, while no characteristic signal for TEMP-$^1O_2$ was detected. This confirmed that H-CNT effectively activated PAA to generate reactive oxygen radicals *via* O–O bond cleavage, without involving $^1O_2$. Notably, the application of an electric field (2.0 V) dramatically enhanced the signal intensities of both DMPO-$HO^{\bullet}$ and DMPO-$RO^{\bullet}$, demonstrating the promoting role of the electric field in facilitating electron transfer and PAA activation.

To quantitatively evaluate the contribution of various reactive species to AN degradation, comprehensive quenching experiments were conducted using multiple specific scavengers (Fig. 2d). The addition of 10 mmol/L *tert*-butanol (TBA), a strong $HO^{\bullet}$ scavenger [27], showed negligible effect on the AN removal. Similarly, methanol (MeOH) only reduced the degradation efficiency to 88.6 %. These results clearly indicated that $HO^{\bullet}$ played a minor role in the EC/H-CNT/PAA system [28]. Furthermore, the introduction of 50 mmol/L L-histidine (L-His) as the $^1O_2$ quencher produced no inhibitory effects [29], excluding $^1O_2$ as a significant contributor to the AN degradation. The role of other radicals in AN degradation was further investigated using 50 mmol/L CH_2BrCl and phenol as specific quenching agents. CH_2BrCl could selectively target surface-associated R–$O^{\bullet}$ species, whereas phenol effectively quenched both surface-bound R–$O^{\bullet}$ and $HO^{\bullet}$ radicals [30]. The introduction of ei-

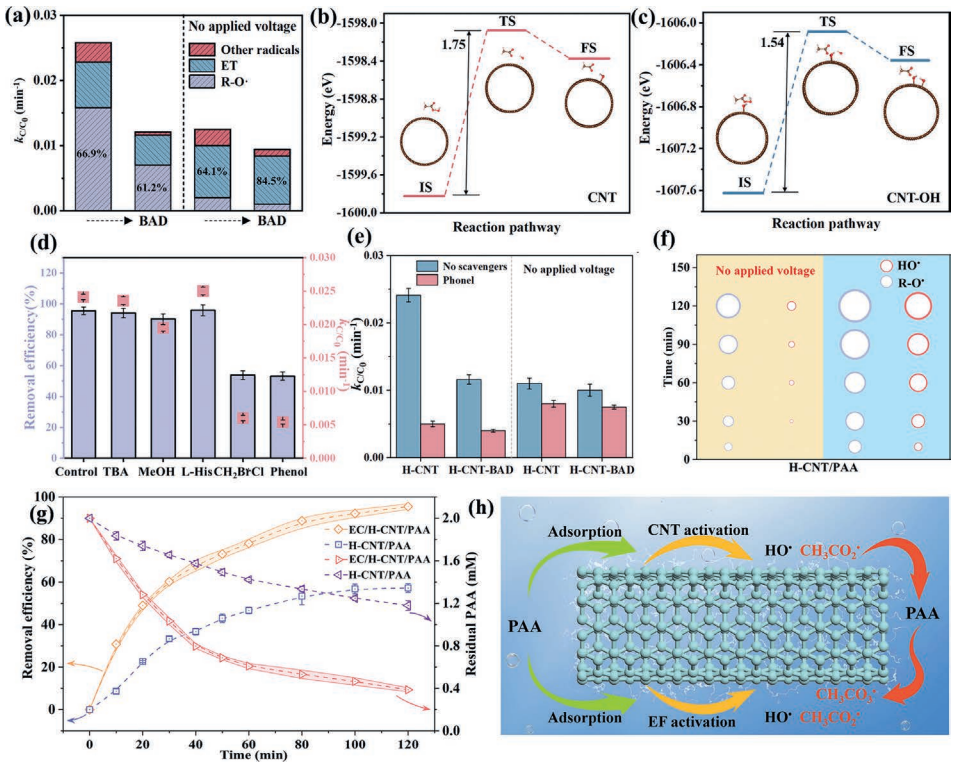


Fig. 2. (a) Open-circuit potential curves for the H-CNT. (b, c) Reaction pathway of the activation of PAA on pristine CNT and CNT–OH, where IS, TS, and FS represent the initial structure, transition structure, and final structure, respectively. (d) Effects of different scavengers on the AN removal. (e) Effect of phenol for AN removal in different systems. (f) Schematic representation of the signal intensity of R-O• and HO• with the change of reaction time. (g) Effect of electric field on removal efficiency of AN and residual PAA concentration in H-CNT/PAA system. (h) Potential pathway of radical formation. Condition: $[AN]_0 = 0.04$ mmol/L, $[PAA]_0 = 2.0$ mmol/L, $[quencher]_0 = 50$ mmol/L, initial pH 7, voltage = 2.0 V, flow rate = 3.0 mL/min.

ther quencher resulted in nearly identical suppression of AN degradation, reducing the removal efficiency from 95.5 % to 53.22 % and 53.10 %, respectively. This parallel inhibitory pattern, where phenol's dual quenching capability provided no additional suppression beyond that achieved by the CH_2BrCl alone, definitively excluded HO• as a significant contributor while confirming surface-bound R–O• as the dominant reactive species governing the AN degradation in the EC/H-CNT/PAA system.

Having identified surface-bound R–O• as the dominant reactive species, we further explored the origin of these radicals and the key factors governing their generation. Based on the previous findings, the application of an electric field emerged as a crucial determinant in shaping the catalytic behavior. As shown in Fig. 2e, quenching surface-bound radicals with phenol posed negligible effect on AN degradation in the absence of an electric field, thereby confirming the dominance of the non-radical electron-transfer pathway under those conditions. However, upon application of an electric field, a dramatic mechanistic shift was observed. The introduction of phenol under electrochemical conditions led to substantial suppression of the degradation reaction, as evidenced by a decrease in the *pseudo*-first-order rate constant from 0.0247 min^{-1} to 0.0052 min^{-1}. This result unambiguously established that surface-bound R–O• radicals became the primary reactive species when the system was electrified, highlighting the dominant role of the electric field in facilitating radical generation. Further confirmation of this electric-field-induced effect was obtained by selectively blocking the C–OH groups on the H-CNT surface using benzoyl anhydride (BAD). In this modified system, the degradation performance was significantly inhibited, and the addition of phenol further reduced the *pseudo*-first-order rate constant from 0.0122 min^{-1} to 0.0039 min^{-1}. This result emphasizes that the C–OH groups are indispensable for the formation of R–O• radicals, and their activation under the electric field is a critical factor in the efficient oxidation of AN. The pivotal role of the electric field in promoting radical formation was also corroborated by the temporal evolution of R–O• radicals (Fig. 2f). In the electrified system, the intensity of surface-bound R–O• increased at a significantly faster rate compared to the non-electrified system. This faster accumulation of radicals in the presence of the electric field further validated the hypothesis that the electric field accelerates the generation of R–O• by influencing the interfacial charge distribution. The underlying mechanism driving this enhancement is two-fold. First, the electric field induced pronounced interfacial charge polarization at the CNT surface, which facilitated electron transfer from PAA to the CNT surface and simultaneously stabilized the key transition state for O–O bond cleavage. This stabilization effectively lowered the activation energy barrier required for the heterolytic fission of PAA, thereby promoting the generation of R–O• radicals. Second, the electric field can also weaken the O–O bond in the PAA molecule adsorbed on the CNT surface by enhancing its polarization, making it more susceptible to scission. This process is analogous to an "electronic catalysis", where the external voltage acts as a trigger to facilitate the heterogeneous activation of PAA, leading to more efficient radical production (Fig. 2g).

Based on the comprehensive experimental evidence, we concluded that the functionalized H-CNT simultaneously operated through two distinct yet cooperative pathways for PAA activation and pollutant degradation (Fig. 2h). The electric-field-enhanced surface-mediated pathway relied on oxygen functional groups particularly C–OH sites (Fig. 3a) to activate PAA forming surface-bound radicals that directly oxidize pollutants. The direct involvement of these C–OH groups is conclusively demonstrated by the post-reaction XPS analysis, which revealed a significant decrease in their

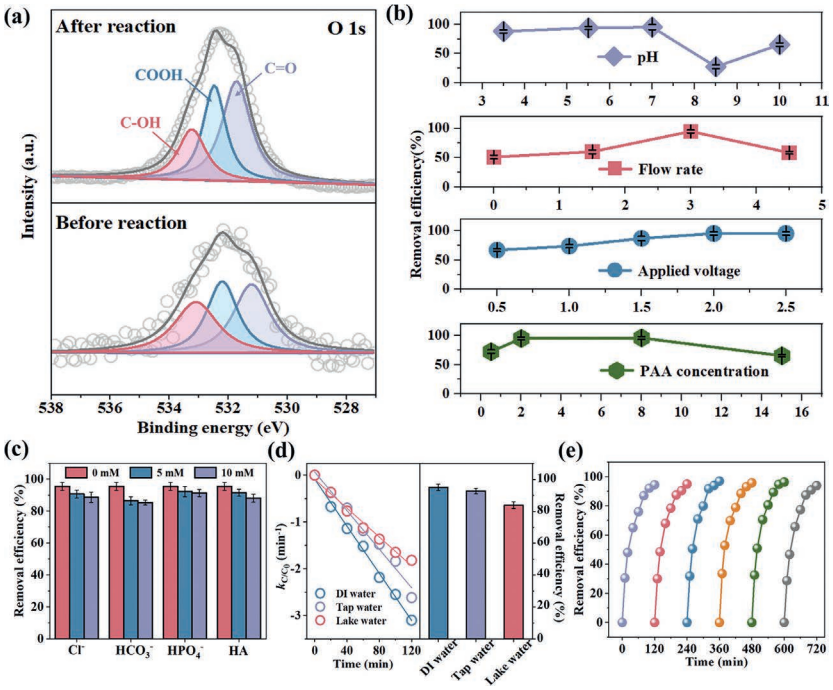


Fig. 3. (a) XPS spectra of O 1s of the H-CNT after and before reaction. (b) Effect of operating parameters (pH, flow rate, applied voltage and PAA concentration) on AN removal. (c) Effects of common inorganic anions and HA for AN removal efficiency. mM = mmol/L. (d) AN removal in different water matrixes in EC/H-CNT/PAA system. (e) Reusability test of H-CNT membrane.

relative proportion from 31.5 % to 22.0 %. Concurrently, the electron transfer pathway utilized the conjugated π system of H-CNT to mediate direct electron shuttling from pollutants to the PAA molecules *via* the H-CNT–PAA* complex. These two pathways collectively enabled efficient AN degradation through complementary oxidation mechanisms.

To optimize the performance of the EC/H-CNT/PAA system, the effects of various operational parameters on the degradation efficiency of AN were systematically investigated. These parameters included the initial pH of the solution, applied voltage, flow rate, and PAA concentration. Each of these factors significantly impacted the system's efficiency and provided insights into the operational dynamics of the system.

The initial pH of the solution plays a critical role in the performance of the EC/H-CNT/PAA system, as it influences the acid-base equilibrium of PAA, which in turn governs the availability of reactive species. As shown in Fig. 3b, the removal efficiency exhibited only a moderate decrease under strong acidic conditions (*e.g.*, 69.6 %) compared to that at neutral conditions (95.5 %), but dropped markedly under alkaline conditions. This trend is governed by the acid-base equilibrium of PAA ($pK_a = 8.2$) [31]. As the pH approaches or exceeds pK_a of 8.2, PAA undergoes self-decomposition (Eqs. 1–3) [18], leading to a significant decline in AN removal. The lowest efficiency observed at pH 8.5 can be explained by the accelerated depletion of PAA near its pK_a. Interestingly, the degradation efficiency recovered to approximately 70 % at pH 10. This rebound can be ascribed to the contribution of alkaline-driven direct oxidation or the formation of different reactive species (*e.g.*, $HO^{\bullet}$ or $O_2^{\bullet-}$) under highly alkaline conditions [32], which partially compensated for the reduced availability of PAA^0.

$$CH_3C(O)OOH + H_2O \rightarrow CH_3C(O)OO^- + H_3O^+ \quad (1)$$

$$CH_3C(O)OOH + CH_3C(O)OO^- \rightarrow CH_3COOH + CH_3CO_2^- + O_2 \quad (2)$$

$$CH_3C(O)OO^- + H_2O_2 \rightarrow CH_3CO_2 + H_2O + O_2 \quad (3)$$

The configuration of the electrochemical reactor also significantly influenced AN removal efficiency. As shown in Fig. 3b, when the system was operated in a batch reactor, the AN removal efficiency reached only 39.7 % after 120 min, which can be attributed to the slow mass transfer of PAA and AN within the reactor, limiting the effective interaction between these species and the H-CNT electrode. In stark contrast, the flow-through filtration mode achieved 82 % removal over the same period, demonstrating the advantage of enhanced mass transport [33]. To further investigate the effect of flow dynamics, a series of experiments at different flow rates (1.5–4.5 mL/min) were conducted to evaluate the influence on AN degradation. As seen from Fig. 3b, when flow rate was increased from 1.5 mL/min to 3.0 mL/min, the AN removal efficiency enhanced from 48.3 % to 95.5 % and reached the plateau. The increased flow rate promoted the circulation of the solution in the system, while on the other hand, it enhanced the effectiveness of convective mass transfer. However, the decreased removal efficiency was observed once the flow rate further increased to 4.5 mL/min, which may be attributed to the declined hydraulic retention time (Text S6 in Supporting information) of PAA and AN in reactor and thus is adverse to the complete degradation of pollutants.

The effect of applied voltage magnitude on the degradation efficiency of AN in the EC/H-CNT/PAA system was also investigated. As shown in Fig. 3b, increasing the voltage from 0.5 V to 2.0 V resulted in a significant enhancement in AN removal, reaching 95.5 %. This improvement was linked to the increased generation of ROS, as demonstrated by enhanced EPR signals under higher voltage. The applied electric field accelerated the activation of PAA, promoting the formation of radicals that are crucial for the degradation of AN. However, when the voltage was increased beyond 2.0 V (to 2.5 V), a slight decrease in removal efficiency was observed, likely due to the onset of side reactions such as oxygen evolution or hydrogen peroxide, which can consume the radicals and reduce their availability for degradation [23].

The concentration of PAA is a critical factor in determining the degradation efficiency, as it directly influences the generation of

reactive oxygen species. As shown in Fig. 3b, when the concentration of PAA increased from 0.5 mmol/L to 2 mmol/L, the removal of AN elevated from 67.5 % to 95.5 %, because a higher PAA concentration led to the production of more ROS. However, no obvious promotion was observed when the concentration rose to 12.5 mmol/L, suggesting that the available active sites on the H-CNT membrane became saturated. A significant inhibition to AN degradation was detected with the concentration of PAA further increased to 15 mmol/L. Previous studies have shown that excessive PAA can weaken the removal efficiency of pollutants by reacting with radicals (Eqs. 4–7), and the decrease of system pH caused by excessive PAA may also be a reason [12].

$$CH_3C(O)OOH + {}^{\bullet}OH \rightarrow CH_3CO^{\bullet} + O_2 + H_2O \quad (4)$$

$$CH_3C(O)OOH + {}^{\bullet}OH \rightarrow CH_3COOH + HO_2{}^{\bullet} \quad (5)$$

$$CH_3C(O)OOH + CH_3C(O)O^{\bullet} \rightarrow CH_3C(O)OO^{\bullet} + CH_3C(O)OH \quad (6)$$

$$CH_3C(O)OO^{\bullet} + H_2O_2 \rightarrow CH_3C(O)OOH + HO_2{}^{\bullet} \quad (7)$$

The stability and practical applicability of the EC/H-CNT/PAA system were evaluated by considering the influence of common ionic components and natural organic matter present in real aquatic environments. These constituents can significantly affect the performance of treatment technologies by either inhibiting or enhancing the degradation process [34]. To assess the robustness of the system in the presence of such compounds, we investigated the effects of Cl^-, $HCO_3{}^-$, $HPO_4{}^{2-}$, and HA on AN degradation. As shown in Fig. 3c, the addition of 10 mmol/L NaCl caused only minor inhibition of AN degradation. The slight inhibition observed can be attributed to a mechanistic interplay. The competitive adsorption of Cl^- on the H-CNT surface likely hinders the direct interaction between PAA and the active C–OH sites, thereby suppressing the primary PAA decomposition pathway. Although Cl^- can be electrochemically converted to active chlorine species (*e.g.,* HClO), its oxidation potential (~1.48 V at neutral pH) is considerably lower than that of the dominant R–O$^{\bullet}$ radicals derived from PAA activation (*e.g.*, $CH_3C(O)O^{\bullet}$, >2.0 V) [35]. Consequently, the limited oxidative capacity and efficiency of the active chlorine species cannot fully compensate for the suppressed PAA activation, resulting in the observed net minor inhibition [36]. Similarly, $HCO_3{}^-$, a well-known scavenger of reactive radicals, exhibited a slight inhibitory effect. This can be attributed to the scavenging of surface-bound R–O$^{\bullet}$ species, leading to the formation of carbonate radicals ($CO_3{}^{\bullet -}$), which exhibit lower reactivity and selectivity toward AN oxidation compared to the primary R–O$^{\bullet}$ radicals [37]. In contrast, $HPO_4{}^{2-}$ showed only a marginal inhibitory effect on the degradation process. Fig. 3c also demonstrated the inhibitory effect of HA on AN removal in the EC/H-CNT/PAA process. When 10 mg/L HA was introduced to the system, AN removal decreased from 95.5 % to 84.7 %. Previous studies have reported relatively high reaction rate constants between R–O$^{\bullet}$ and HA ($k = 1 \times 10^4$ L mg^{-1} s^{-1}) [18]. Additionally, HA may compete with both AN and PAA for electrons, thereby inhibiting both the PAA activation process and direct electron transfer between AN and the CNT electrode.

Despite these challenges, the EC/H-CNT/PAA system maintained effective AN removal performance in complex water matrices. The basic water quality parameters for the different water matrices are presented in Table S2 (Supporting information). As shown in Fig. 3d, when tap water and lake water were used as background matrices, the system still achieved AN removal efficiency exceeding 82 %, demonstrating its adaptability to complex aqueous environments. Importantly, the proposed electrochemical filtration process required an energy consumption of only 0.033 kWh/m^3 (Text S7 in Supporting information) at the voltage of 2.0 V, which was comparable to or even lower than various state-of-the-art technologies [38,39]. Furthermore, the system exhibited excellent operational stability through six consecutive treatment cycles with virtually no decline in performance (Fig. 3e). The average AN removal efficiency remained at 95.8 %, confirming the robust stability of the system for continuous operation.

In addition to evaluating its stability in complex matrices, the EC/H-CNT/PAA system's versatility was assessed by testing its ability to degrade various organic micropollutants. As shown in Fig. S9 (Supporting information), the system demonstrated excellent removal efficiency (>90 %) for several typical electron-rich pollutants, including SMX, BPA, and TC. In contrast, significantly lower removal efficiencies were observed for electron-deficient pollutants such as BA (35.1 %) and NB (27.5 %). This selectivity can be attributed to the preferential reactivity of R-O$^{\bullet}$ radicals towards electron-rich compounds, as previously established.

Moreover, a life cycle assessment was conducted to benchmark the environmental performance of the proposed system against an electro-activation PDS system (Figs. 4a and b, Text S8 and Table S3 in Supporting information) [40]. The results demonstrated a clear environmental advantage of the proposed system across 18 impact categories evaluated. As illustrated in Figs. 4a and b, the proposed system yielded significantly lower impact potentials. Key reductions included a 19.7 % decrease in global warming potential (GWP), a 27.1 % reduction in fossil fuel consumption (FFP), and a 29.1 % mitigation of particulate matter formation potential (PMFP). Substantial improvements were also achieved in toxicity-related impacts, with reductions of approximately 25 % in both carcinogenic and non-carcinogenic human toxicity potential (HTPc & HTPnc). Furthermore, the risks of acidification and eutrophication were notably lower, with terrestrial acidification potential (TAP) and freshwater eutrophication potential (FEP) reduced by 19.6 % and 29.9 %, respectively. These comprehensive reductions, observed without any burden-shifting to other environmental issues, are primarily attributed to the system's higher efficiency and optimized material utilization, confirming its superior environmental profile.

To evaluate the antifouling capability of the H-CNT membrane, HA was employed as a representative natural organic matter to simulate membrane fouling in natural aquatic environments [41]. Filtration tests (Fig. S10a and Text S9 in Supporting information) revealed that a simple rinsing process achieved a flux recovery rate of 60 %. In contrast, when an electro-assisted self-cleaning process with a PAA solution was applied, the flux recovery rate was significantly enhanced to 96 %, demonstrating outstanding fouling resistance. This remarkable performance was further elucidated by the XDLVO theory. As illustrated in Fig. S10b and Text S10 (Supporting information), the H-CNT membrane exhibited a significantly higher positive total interfacial interaction energy, which underscores its superior thermodynamic repulsion and antifouling potential against natural organic matter.

These results underscore the potential of the EC/H-CNT/PAA system for practical, sustainable wastewater treatment. The system not only provides efficient degradation of a range of organic pollutants but also demonstrates stability and adaptability in complex water environments, making it a promising candidate for real-world applications.

To elucidate the transformation mechanism of AN, the reaction intermediates were identified, and potential degradation pathways were proposed. As illustrated in Fig. S11 (Supporting information), the degradation proceeds through three competing pathways initiated by distinct reactive species. In the pathway 1, the amino group in AN was initially attacked by radicals to form nitrosobenzene, which was further oxidized to nitrobenzene. Subsequent ring opening of nitrobenzene yields maleic acid. Pathway 2 began with hydroxyl substitution at the amino *para*-position of

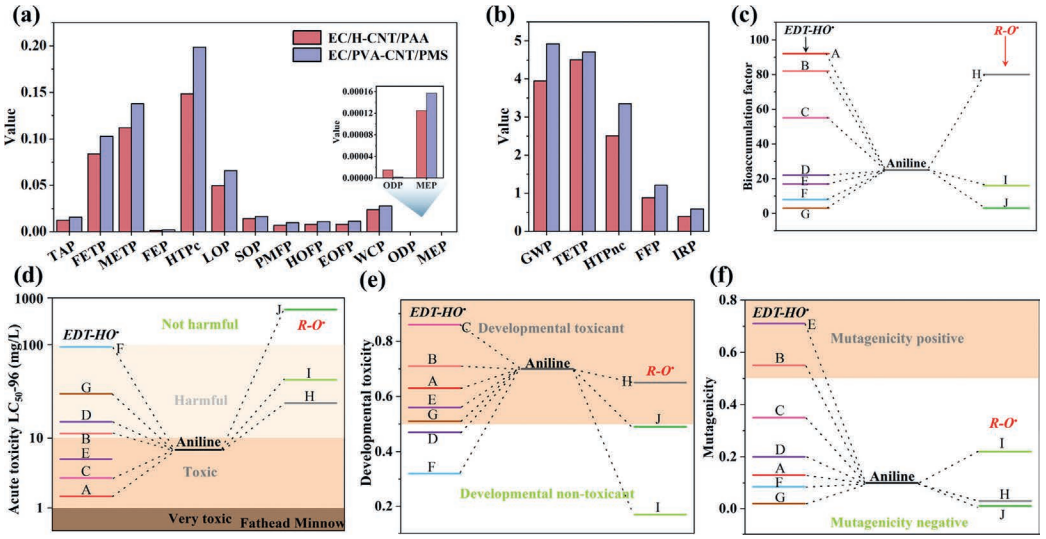


Fig. 4. (a, b) Comparative environmental impact assessment of two systems, considering TAP, FETP, GWP, and other 15 impact categories. (c) Bioaccumulation factor, (d) acute toxicity (Fathead minnow), (e) developmental toxicity, and (f) mutagenicity of AN and its degradation intermediates in H-CNT/PAA and EC/H-CNT/PAA systems.

the benzene ring, forming *p*-hydroxyaniline. Then *p*-hydroxyaniline was attacked by radicals to form *para*-aminobenzoquinone and further converted to *p*-benzoquinone, which underwent ring cleavage to form maleic acid. In the pathway 3, AN first reacts with HO• to produce *p*-aminophenol through radical addition reaction. Next, HO• continues to react with *p*-aminophenol through hydrogen atom abstraction to generate *p*-aminobenzoquinone and further transformed into *p*-benzoquinone. Finally, *p*-benzoquinone transformed into maleic acid *via* ring opening reaction and further decomposed to carbon dioxide and water.

Furthermore, this study evaluated the toxicity of intermediate products generated during AN degradation using four key indicators, including bioaccumulation factor, developmental toxicity, mutagenicity, and acute toxicity (Text S11 in Supporting information). As illustrated in Figs. 4c–f, most intermediates exhibited lower developmental toxicity than the parent AN, except for product C. Acute toxicity, represented by the median lethal concentration, also showed significant reduction in all intermediates except products A and H. Similarly, the teratogenic potential and bioaccumulation tendency of AN were effectively suppressed after degradation. Notably, the intermediates formed *via* the R–O•-mediated pathways generally demonstrated lower toxicity compared to those generated through HO• or electron transfer pathways. These findings confirmed that the EC/H-CNT/PAA system not only efficiently degrades AN but also significantly reduces its ecological impact by steering the reaction toward less toxic transformation products.

In conclusion, this study demonstrated an integrated electrochemical filtration system featuring a metal-free CNT membrane for highly efficient AN degradation through synergistic PAA activation. The introduced electric field (2.0 V) fundamentally shifted the dominant mechanism from a non-radical electron-transfer pathway to a surface radical-mediated process, with C–OH groups identified as the primary active sites. Kinetic analysis confirmed a notable synergy, with the EC/H-CNT/PAA system exhibiting a pseudo-first-order rate constant of 2.41×10^{-2} min^{-1}, which is 12.7 and 2.3 times higher than those of the electrochemical and catalytic systems alone. Under optimized conditions, the system achieved 95.5 % AN removal within 120 min, maintained over 90 % efficiency over six consecutive cycles, and demonstrated robust performance (>82 % removal) across diverse real water matrices. The combined anti-fouling and XDLVO analysis further revealed the exceptional stability and fouling resistance of the H-CNT membrane. Most importantly, life cycle assessment and toxicity analysis verified the superior environmental profile of this technology, highlighting significant reductions in global warming potential and ecotoxicity. By rationally combining electrochemistry, membrane technology, and functional nano-catalysis, this work provides both mechanistic insight into carbon-catalyzed PAA activation and a practical, sustainable strategy for the treatment of refractory organic wastewater.

CRediT authorship contribution statement

Wentian Zheng: Writing – original draft, Data curation. **Jiachen Wang:** Validation, Investigation. **Yifan Ren:** Writing – review & editing, Formal analysis. **Yanbiao Liu:** Supervision, Funding acquisition, Conceptualization.

Declaration of competing interest

The authors declare that they have no known competing financial interests or personal relationships that could have appeared to influence the work reported in this paper.

Acknowledgments

This work was supported by the Fundamental Research Funds for the Central Universities and Graduate Student Innovation Fund of Donghua University (No. CUSF-DH-D-2024032), the Natural Science Foundation of Shanghai (No. 23ZR1401300), and the National Natural Science Foundation of China (No. W2412093).

Supplementary materials

Supplementary material associated with this article can be found, in the online version, at doi:10.1016/j.cclet.2026.112462.

References

[1] P. Vitale, P.B. Ramos, V. Colasurdo, et al., J. Clean. Prod. 206 (2019) 1041–1050.
[2] S. Wang, M.R. Razanajatovo, X. Du, et al., Chin. Chem. Lett. 35 (2024) 109140.
[3] S. Wang, S. Guo, X. Du, et al., Chem. Eng. J. 495 (2024) 153604.
[4] W. Ren, C. Cheng, P.H. Shao, et al., Environ. Sci. Technol. 56 (2022) 78–97.
[5] X.G. Duan, H.Q. Sun, S.B. Wang, Acc. Chem. Res. 51 (2018) 678–687.
[6] W.P. da Silva, T.D. Carlos, G.S. Cavallini, et al., Water Res. 168 (2020) 115143.
[7] J.W. Wang, Z.P. Wang, Y.J. Cheng, et al., Water Res. 201 (2021) 117291.
[8] M.Q. Cai, P.Z. Sun, L.Q. Zhang, et al., Environ. Sci. Technol. 51 (2017) 14217–14224.
[9] J.W. Wang, Y. Wan, J.Q. Ding, et al., Environ. Sci. Technol. 54 (2020) 14635–14645.

[10] X.J. Bai, S. Qin, H.M. Liu, et al., Chem. Eng. J. 524 (2025) 169624.
[11] J. Kim, T.Q. Zhang, W. Liu, et al., Environ. Sci. Technol. 53 (2019) 13312–13322.
[12] J. Kim, P.H. Du, W. Liu, et al., Environ. Sci. Technol. 54 (2020) 5268–5278.
[13] F. Chen, L.L. Liu, J.J. Chen, et al., Water Res. 191 (2021) 116799.
[14] D.L. Guo, Y. Yao, S.J. You, et al., Appl. Catal. B: Environ. 309 (2022) 121289.
[15] F.Y. Zhou, C. Lu, Y.Y. Yao, et al., Chem. Eng. J. 281 (2015) 953–960.
[16] D.Z. Kong, Y.M. Zhao, X.R. Fan, et al., Environ. Sci. Technol. 56 (2022) 11707–11717.
[17] D.Z. Kong, Y.M. Zhao, H.D. Guo, et al., ACS EST Eng. 3 (2023) 1030–1041.
[18] D.L. Yuan, K. Yang, S.Y. Pan, et al., Sep. Purif. Technol. 276 (2021) 119317.
[19] C.Y. Nie, Z.M. Ao, X.G. Duan, et al., Chemosphere 206 (2018) 432–438.
[20] J.L. Peng, Y.L. He, C.Y. Zhou, et al., Chin. Chem. Lett. 32 (2021) 1626–1636.
[21] D.L. Guo, Y.B. Liu, H.D. Ji, et al., Environ. Sci. Technol. 55 (2021) 4045–4053.
[22] T.C. Liu, S.Z. Xiao, N. Li, et al., Nat. Commun. 14 (2023) 2881.
[23] W.T. Zheng, S.J. You, Y. Yao, et al., Engineering 30 (2023) 144–152.
[24] S.Y. Chen, T. Luo, K.J. Chen, et al., Angew. Chem. Int. Ed. 60 (2021) 16607–16614.
[25] F. Miao, X.T. Yue, C. Cheng, et al., Water Res. 227 (2022) 119346.
[26] P.P. Zhang, Y.Y. Yang, X.G. Duan, et al., ACS Catal. 11 (2021) 11129–11159.
[27] R.Y. Xiao, Z.H. Luo, Z.S. Wei, et al., Chin. Chem. Lett. 37 (2026) 111853.
[28] Z. Liu, H. Ding, C. Zhao, et al., Water Res. 159 (2019) 111–121.
[29] B.K. Huang, Z.L. Wu, J. Zhang, et al., Chin. Chem. Lett. 37 (2026) 111537.
[30] L. Wang, X. Lan, W. Peng, et al., J. Hazard. Mater. 408 (2021) 124436.
[31] W.P. Kwan, B.M. Voelker, Environ. Sci. Technol. 37 (2003) 1150–1158.
[32] J.L. Wang, S.Z. Wang, Chem. Eng. J. 334 (2018) 1502–1517.
[33] Y.B. Liu, G.D. Gao, C.D. Vecitis, Acc. Chem. Res. 53 (2020) 2892–2902.
[34] Z. Zhao, Y. Mi, S. Wang, et al., Water Res. 280 (2025) 123510.
[35] S. Liang, L. Zhu, J. Hua, et al., Environ. Sci. Technol. 54 (2020) 6406–6414.
[36] S. Chen, M.Q. Cai, Y.Z. Liu, et al., Water Res. 150 (2019) 153–161.
[37] W.T. Zheng, Y.B. Liu, W. Liu, et al., Water Res. 194 (2021) 116961.
[38] A. Farhat, J. Keller, S. Tait, et al., Environ. Sci. Technol. 49 (2015) 14326–14333.
[39] A. Farhat, J. Keller, S. Tait, et al., Electrochem. Commun. 89 (2018) 14–18.
[40] C. Nie, Z. Ao, X. Duan, et al., Chemosphere 206 (2018) 432–438.
[41] Q. Zeng, Z. Zhao, Y. Wang, et al., Chem. Eng. J. 522 (2025) 167962.